

1
2
3
4
5
6
7
8
9
10
11
12
13
14
15
16
17
18
19
20
21

The role of spatial scale and background climate in the latitudinal temperature response to deforestation

Yan Li^{1,2,3,4}

Nathalie De Noblet-Ducoudré⁵

Edouard L. Davin⁶

Safa Motesharrei^{4,7,8}

Ning Zeng²

Shuangcheng Li^{1,3}

Eugenia Kalnay^{2,4}

1. College of Urban and Environmental Sciences, Peking University, Beijing 100871, China.
2. Department of Atmospheric and Oceanic Science, University of Maryland, College Park, Maryland 20742, USA.
3. Key Laboratory for Earth Surface Processes of The Ministry of Education, Peking University, Beijing 100871, China.
4. The Institute for Physical Science and Technology, University of Maryland, College Park, Maryland 20742, USA.
5. Laboratoire des Sciences du Climat et de l'Environnement, Institut Unité Mixte CEA-CNRS-UVSQ, Université Paris-Saclay, Orme des Merisiers Bât. 712, 91191 Gif-sur-Yvette, France

- 22 6. Institute for Atmospheric and Climate Science, Eidgenössische Technische
23 Hochschule (ETH) Zurich, 8092 Zürich, Switzerland
- 24 7. Department of Physics, University of Maryland, College Park, Maryland 20742,
25 USA.
- 26 8. National Socio-Environmental Synthesis Center (SESYNC), Annapolis, Maryland,
27 21401

28

29

30

31 Correspondence email: yanli.geo@gmail.com

32

33

34

35

36

37

38

39

40

41

Abstract:

42 Previous modeling and empirical studies have shown that the biophysical impact of
43 deforestation is to warm the tropics and cool the extra-tropics. In this study, we use an
44 earth system model of intermediate complexity to investigate how deforestation at
45 various spatial scales affects ground temperature, with an emphasis on the latitudinal
46 temperature response and its underlying mechanisms. Results show that the latitudinal
47 pattern of temperature response depends non-linearly on the spatial extent of
48 deforestation and the fraction of vegetation change. Compared with regional
49 deforestation, temperature change in global deforestation is greatly amplified in
50 temperate and boreal regions, but is dampened in tropical regions. Incremental forest
51 removal leads to increasingly larger cooling in temperate and boreal regions, while the
52 temperature increase saturates in tropical regions. The latitudinal and spatial patterns of
53 the temperature response are driven by two processes with competing temperature effects:
54 decrease in absorbed shortwave radiation due to increased albedo and decrease in
55 evapotranspiration. These changes in the surface energy balance reflect the importance of
56 the background climate on modifying the deforestation impact. Shortwave radiation and
57 precipitation have an intrinsic geographical distribution that constrains the effects of
58 biophysical changes and therefore leads to temperature changes that are spatially varying.
59 For example, wet (dry) climate favors larger (smaller) evapotranspiration change, thus
60 warming (cooling) is more likely to occur. Our analysis reveals that the latitudinal
61 temperature change largely results from the climate conditions in which deforestation
62 occurs, and is less influenced by the magnitude of individual biophysical changes such as
63 albedo, roughness, and evapotranspiration efficiency.

64 **1. Introduction**

65 Forests play a critical role in regulating climate through both biogeochemical and
66 biophysical processes. Deforestation, driven by anthropogenic activities either directly,
67 e.g., agriculture expansion, or indirectly, e.g., climate change induced disturbance (Allen
68 *et al.*, 2010), can result in changes in earth's radiation balance, hydrological cycle, and
69 atmospheric composition (Bonan, 2008). Deforestation is a major land conversion that
70 has taken place historically over large scales and continues to be prevalent in the 21th
71 century (Hansen *et al.*, 2013).

72 Previous climate model studies highlight the interesting observation that temperature
73 response to deforestation appears to depend on latitude (Davin & de Noblet-Ducoudré,
74 2010). For example, large-scale deforestation in the tropics leads to temperature increase
75 (Nobre *et al.*, 1991; Snyder *et al.*, 2004; Davin & de Noblet-Ducoudré, 2010) mostly due
76 to the strong warming effect associated with reduced evapotranspiration. However, forest
77 removal in the temperate and high-latitude regions results in surface temperature decrease.
78 This decrease is explained by the dominant mechanism, albedo, which increases in the
79 cleared land and leads to lower shortwave radiation absorption (Bounoua *et al.*, 2002;
80 Snyder *et al.*, 2004). This albedo-induced cooling effect is particularly strong in the
81 boreal regions where the snow mask effect is involved (Bonan *et al.*, 1992, 1995). In
82 agreement with the climate model experiments, empirical studies using in-situ air
83 temperature (Lee *et al.*, 2011; Zhang *et al.*, 2014) and satellite-derived land surface
84 temperature (Li *et al.*, 2015) also show that the temperature effects of forests have a clear
85 latitudinal pattern.

86 Compared with biogeochemical effects, i.e., release of CO₂ to the atmosphere that
87 warms the global climate, biophysical effects are more heterogeneous, most strongly felt
88 at regional and local levels (Bala *et al.*, 2007; Pitman *et al.*, 2012), and vary with season
89 and location (Snyder *et al.*, 2004; Betts *et al.*, 2007, Li *et al.*, 2015). It is thought that
90 biophysical effect, especially albedo and evapotranspiration, are major biophysical
91 mechanisms through which deforestation affects temperature in latitudinal patterns
92 (Gibbard *et al.*, 2005). However, due to the high spatial variability of biophysical
93 properties, the dominant mechanism and the net effect of deforestation could vary by
94 particular location. This is further complicated by the influence of specific location's
95 background climate on the altered water and energy balance. For example, previous
96 studies show that climate conditions, such as snow and rainfall, can enhance or dampen
97 biophysical effects (Pitman *et al.*, 2011; Li *et al.*, 2015). Such complexity is reflected in
98 temperate forests, where the two biophysical mechanisms with opposite effects cancel
99 each other, making their net effect much more uncertain compared to other forests. This
100 incomplete understanding of temperate forests was confirmed by the mixed results
101 obtained from modeling and observational studies (Bonan, 2008; Wickham *et al.*, 2013;
102 Li *et al.*, 2015). Further complication comes from deforestation-triggered changes in
103 other energy components (such as sensible heat) and multiple atmospheric feedbacks that
104 can modify the albedo and evapotranspiration impact. Therefore, it is important to further
105 investigate the relative strength of albedo and evapotranspiration impact on temperature
106 change, and how much those factors are influenced by the interaction with the local
107 climate and other factors.

108 In addition to these biophysical effects, the spatial scale of deforestation is also an
109 important factor in climatic impact. It has been shown that both spatial extent (global-
110 regional-local) and degree of vegetation change (partial disturbance to complete removal)
111 can alter the impact of deforestation (Sampaio *et al.*, 2007; Longobardi *et al.*, 2012).
112 Evidence for this behavior is seen in the Amazon area, where depending on the spatial
113 scale of deforestation, precipitation change can either exhibit a linear or non-linear
114 relationship with vegetation change (Avissar *et al.*, 2002; Baidya Roy & Avissar, 2002;
115 Souza & Oyama, 2010). And this relationship could even become opposite in sign
116 (Runyan, 2012). The effect of vegetation change at various scales is still not clear on
117 either the scale-dependency or latitudinal pattern of temperature response.

118 As described, the impact on temperature as a result of deforestation originates from
119 the altered biophysical properties such as albedo, roughness, canopy conductance, surface
120 emissivity, etc. The magnitude of some of these alterations, as well as their impact on
121 temperature, may have inherent latitudinal patterns. For instance, the difference in albedo
122 between forest and open land increases with latitude (Li *et al.*, 2015). By investigating
123 how changes to several biophysical properties contribute to temperature change, we can
124 better understand whether the latitudinal temperature response to deforestation is either
125 directly due to these changes, or the processes that translate these changes to the surface
126 climate response. Efforts have been made to quantify the contribution of each biophysical
127 factor, including both empirical (Juang *et al.*, 2007) and modeling studies (Lean &
128 Rowntree, 1997; Maynard & Royer, 2004; Davin & de Noblet-Ducoudré, 2010) that
129 enable us to decompose the temperature change into components. Such studies can

130 improve our knowledge on the mechanisms for the climate impact induced by vegetation
131 change.

132 In this study, we use an earth system model of intermediate complexity (EMIC) to
133 investigate how deforestation affects temperature through biophysical changes and also
134 examine which physical mechanisms are responsible for the latitude-dependent
135 temperature response (Section 2). To this aim, we first analyze latitudinal temperature
136 changes in response to multiple deforestation scenarios by varying both spatial extent and
137 deforestation fraction (Section 3.1 and 3.2). Next, we explore the possible causes for the
138 latitudinal and spatial pattern of temperature change from both the surface energy balance
139 (Section 3.3), as well as the background climate (Section 3.4). Finally, we show how
140 different biophysical mechanisms affect temperature change and discuss their
141 contributions to the latitudinal pattern (section 3.5). A brief discussion and summary are
142 provided in Section 4.

143 **2. Method**

144 **2.1 Model description**

145 The UMD (University of Maryland) EMIC (Zeng, 2004) is used to perform the
146 experiments. It consists of the global version of QTCM (Quasi-Equilibrium Tropical
147 Circulation Model) atmosphere model (Neelin & Zeng, 2000), the physical land surface
148 model Sland (Simple-land) (Zeng *et al.*, 2000), the dynamic vegetation and carbon model
149 VEGAS (VEgetation-Global-Atmosphere-Soil) (Zeng, 2003; Zeng *et al.*, 2005), and a
150 slab ocean model in which we use prescribed sea surface temperatures (SSTs) in our
151 experiments.

152 Sland is a land surface model of intermediate complexity that is more complicated
153 than the bucket model in its parameterization of evapotranspiration processes, aiming to
154 model the first-order effects relevant to climate simulation. In this model, vegetation
155 parameters such as leaf area index, roughness, stomatal conductance, and vegetation
156 fraction depend on climate and are calculated by VEGAS. For surface albedo, seasonal
157 climatology obtained from satellite is used as inputs (Darnell *et al.*, 1992). Vegetation-
158 albedo feedback is treated in the model by introducing albedo anomalies. This procedure
159 sums the albedo change due to vegetation change (calculated by VEGAS using an
160 empirical formula as a function of leaf area index (LAI)), and the observed albedo
161 climatology used by the atmospheric radiation module (Zeng & Yoon, 2009). This albedo
162 anomalies treatment prioritizes the capture of the first-order effects of albedo change due
163 to vegetation change, since many of the possible processes that are responsible for the
164 observed albedo are difficult to model mechanistically.

165 It should be mentioned that Sland in its current setup does not explicitly account for
166 surface snow, thus no snow-albedo feedback is included. This potentially leads to an
167 underestimation of albedo change in regions with frequent snow. However, it also offers
168 a unique opportunity to examine mechanisms other than snow in the temperature
169 response to deforestation at high latitudes.

170 The VEGAS model simulates the dynamics of vegetation growth and competition
171 among four plant functional types (PFTs): broadleaf tree, needleleaf tree, cold grass, and
172 warm grass. The phenology of these plants is simulated dynamically as the balance
173 between growth and respiration/turnover. The vegetation component is coupled to land
174 and atmosphere through soil moisture dependence of photosynthesis and

175 evapotranspiration, as well as dependence on temperature, radiation, and atmospheric
176 CO₂. The UMD EMIC has been used to study the climate and vegetation feedbacks (e.g.,
177 Zeng *et al.*, 1999; Zeng & Neelin, 2000; Hales *et al.*, 2004; Zeng & Yoon, 2009) and
178 contributed to C⁴MIP, the Coupled Climate–Carbon Cycle Model Intercomparison
179 Project, C⁴MIP (Friedlingstein *et al.*, 2006).

180

181 **2.2 Experiment design**

182 UMD earth system model is a fully coupled model, but the setup for this study is an
183 atmosphere-land-vegetation coupled version with prescribed ocean SST, and CO₂
184 concentration at the preindustrial level of 280 ppm, run at a resolution of 5.625° × 3.75°.
185 The model is driven by a climatological seasonal cycle of SST derived from HadSST
186 (Rayner *et al.*, 2006), averaged over 1960–1990 to smooth the influence of inter-annual
187 climate variability. The model is first run for 500 years to allow for spin-up time during
188 which vegetation is dynamically computed and reaches an equilibrium state with climate.
189 Figure S1 shows the potential vegetation map obtained by the end of model spin-up. The
190 vegetation map generally has a reasonable geographical distribution but does not
191 perfectly match modern vegetation of the real world. This is expected because the
192 potential vegetation is derived from an equilibrium state with climate. Therefore, any
193 differences in the simulated climate compared to modern climate or any simulation bias,
194 for example, in precipitation (Figure S2), could influence the vegetation distribution. In
195 addition, some bias in simulated climate is expected for a model with intermediate
196 complexity. Such bias is tolerable in our experiments due to the focus on the climate
197 response to vegetation change and its mechanisms as opposed to an accurate reproduction

198 of historical climate change. For our analysis, the climatology over the last 10 years of
 199 spin-up is used as the control experiment (CTL). This is adequate for our simulation
 200 because of the small inter-annual variability in the model.

201 Deforestation is imposed by setting the forest fraction in a given grid cell to the
 202 experimental value of either zero or a percentage of its original vegetation. This replaces
 203 the forest with bare soil, as is seen in several previous studies (Bonan *et al.*, 1992;
 204 Gibbard *et al.*, 2005; Snyder, 2010). An alternative strategy of implementing
 205 deforestation experiment is to replace trees with grass (crop). This is considered to be
 206 more “realistic” than replacing trees with bare ground (Davin & de Noblet-Ducoudré,
 207 2010). The conversion of trees to grass is expected to induce a similar but less
 208 pronounced impact on climate (Gibbard *et al.*, 2005), compared to the conversion of trees
 209 to bare ground which would represent the maximum impact of deforestation. Despite this
 210 difference, both strategies are frequently used in existing literature to represent
 211 deforestation, and they yield consistent findings as the operating mechanisms and
 212 feedbacks are the same. In the simulation for deforestation experiment, modified
 213 vegetation fractions are fixed so that the vegetation model becomes “static” rather than
 214 “dynamic”.

Table 1. Deforestation experiment design

Group	I. Spatial extent	II. Deforestation fractions	III. Biophysical factors
Experiment	<ul style="list-style-type: none"> • Tropical • Temperate • Boreal • Global 	<ul style="list-style-type: none"> • 25% global forest removal • 50% global forest removal • 75% global forest removal • 100% global forest removal 	<ul style="list-style-type: none"> • Albedo • Roughness • Evapotranspiration efficiency

215

216 Three groups of experiments are designed to study different aspects of the
217 deforestation impact (Table 1): (I) deforestation with different spatial extents (II) with
218 different deforestation fractions; (III) with individual biophysical factors changed
219 separately. The first two groups address the spatial scale problem for the climatic
220 response to deforestation. Group (I) consists of three regional deforestation scenarios that
221 take place in the tropical (20°S-20°N), northern temperate (20°N-50°N) and boreal
222 (50°N-90°N) regions, and one global deforestation scenario in which all forests are
223 cleared. Group (II) consists of four global deforestation experiments in which forest
224 fractions are reduced as a percent to its original coverage at 25% to 100%. The 100%
225 clearing creates the same experiment as the global deforestation in group I, labeled ALL.

226 Group (III) is designed to separate the effect of individual biophysical factors by
227 which deforestation affects climate. Inspired by Davin & de Noblet-Ducoudre (2010),
228 three experiments are devised to quantify the impact from changes in albedo, roughness,
229 and evapotranspiration efficiency. Our experiment for albedo and roughness differs from
230 Davin & de Noblet-Ducoudre (2010), who compared the case with only “one factor
231 changed” with the case of “everything unchanged”. In contrast, we ultimately compare
232 the case of “everything changed with one factor unchanged” with the case of “everything
233 changed”. Our experiments include global deforestation with albedo unchanged in
234 “noALB”, roughness unchanged in “noRGH”, and evapotranspiration efficiency effect
235 isolated in “EVA”. In noALB experiment, albedo change induced by forest removal is
236 not passed to the atmosphere, which means “no albedo change” indeed in the atmosphere
237 model since it intakes observed albedo data. The other biophysical variables are still
238 being affected by deforestation. Thus, the albedo effect can be isolated by calculating the

239 difference (ALL – noALB) between the regular global deforestation simulation (ALL)
240 that includes the albedo change and the noALB experiment. In noRGH experiment,
241 roughness is set to be unaffected by forest clearing, therefore, the difference ALL -
242 noRGH can be attributed to the roughness effect. The calculation of evapotranspiration
243 involves many parameters. For example, both albedo and roughness can affect ET.
244 Therefore, for EVA experiment, a different strategy is adopted by fixing both albedo and
245 roughness (as in CTL) while other variables are allowed to change. Thus, the difference
246 of EVA and control, EVA - CTL, reflects processes other than albedo and roughness that
247 can affect ET, representing the pure hydrological effect of deforestation that refers to the
248 ability of vegetation to transfer water from the soil to the atmosphere (Davin & de
249 Noblet-Ducoudré, 2010).

250 All deforestation simulations are initialized with the restart files after spin-up whose
251 vegetation map, relevant parameters, and model codes have been modified as described
252 above. Each simulation is run for 100 years and the averaged results of the final 10 years
253 are used for the analysis. Ground temperature is used to analyze temperature change,
254 because the model does not output the 2-m air temperature. Ground temperature has a
255 strong signal of the locally induced temperature change, which is closely coupled to the
256 surface energy balance. This enables us to focus on the local and regional impacts of
257 vegetation change. Only model grid points with forest fractional change larger than 0.1
258 are analyzed for robustness. The resulting changes in LAI, albedo, and roughness,
259 induced by global deforestation, are provided in Supplementary Information (Figure S3–
260 S5).

261

3. Results

3.1 Latitudinal temperature change in response to deforestation

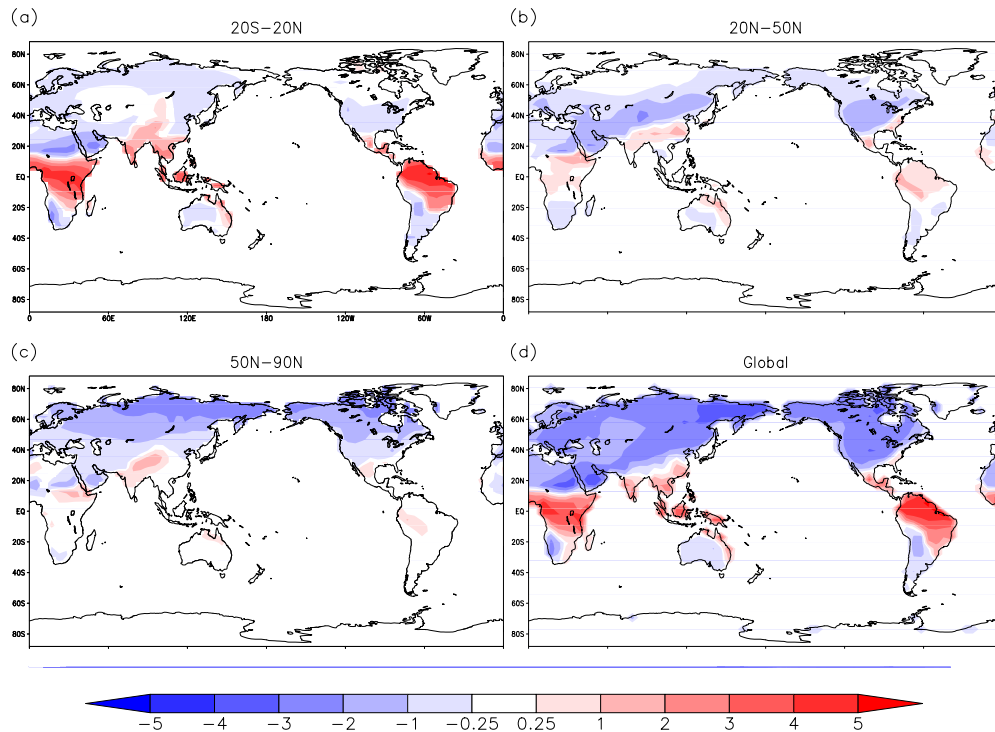


Figure 1. Ground temperature change for (a) tropical (20°S - 20°N), (b) northern temperate (20°N - 50°N), (c) boreal (50°N - 90°N), and (d) global (90°S - 90°N) deforestation (Unit: K)

The latitude-dependence of temperature response is confirmed by the three regional

deforestation experiments (see Figure 1a-c for tropical, northern temperate and boreal,

and Figure 1d for global deforestation experiments). The deforestation impact in the

simulation is a very strong signal relative to the small inter-annual variability, making

almost all changes over the land statistically significant. Therefore, significance levels are

not shown on the map. In tropical deforestation (20°S - 20°N) experiment, a significant

271 and widespread warming is observed over deforested regions by 2.22 K (Table 2),
272 greatest (~4 K) in the Amazon and Central Africa regions and about 1-2 K in South Asia
273 and the east coast of Australia. Although warming is the dominant effect, there are areas
274 around Sahel, North Africa in which we observe cooling up to -2 K. This suggests
275 temperature response can differ within a latitude band, as shown in earlier studies
276 (McGuffie *et al.*, 1995; Snyder *et al.*, 2004). The regional difference is partly due to the
277 regional circulation patterns being affected differently by deforestation (McGuffie *et al.*,
278 1995). Temperature outside the deforestation boundary (e.g., South Asia, North Canada)
279 is also influenced by the tropical deforestation, indicating that the vegetation disturbance
280 signal can spread to distant regions through atmospheric processes. Replacing forest with
281 bare ground leads to a surface albedo increase of 0.26, and a decrease of shortwave
282 absorption at the surface by 38 W/m². Precipitation and evapotranspiration also decline
283 drastically by 3.75 and 2.93 mm/day, respectively, while sensible heat increases.
284 Reducing cloud cover results in an increase in downward shortwave and a decrease in
285 downward longwave radiation (Table 2).

286 In the northern temperate region (20°N-50°N), deforestation causes a temperature
287 decrease of -0.84 K over most areas. North China and most parts of the United States
288 show the largest cooling (~-1.5 K) while a weaker cooling (< -1 K) is observed in Europe.
289 Nevertheless, temperature rise can be found in some areas like South China (1~2K) and
290 Southeast U.S. (~1 K), similar to the tropics. The regional difference also reflects the
291 different response of the surface energy balance to deforestation, and is related to the
292 background climate as discussed in the next section. Other changes, including increased
293 albedo and decreased shortwave absorption as well as decrease in ET and precipitation,

294 can be seen in temperate deforestation, but the magnitudes are much smaller than those in
 295 the tropics. Unlike the tropical region, sensible heat decreases in the temperate region and
 296 is consistent with the sign of temperature change.

297 Compared with the temperate region, deforestation in the boreal region results in a
 298 stronger cooling of -1.70 K but changes in the surface energy components are much
 299 smaller. It should be noted that albedo only increases by 0.22 because of no snow-
 300 masking effect in the land surface model, which could enhance the cooling signal by
 301 amplifying the albedo change. Nevertheless, a considerable cooling is seen in our results
 302 without the snow-masking effect, suggesting that other changes rather than snow
 303 contribute to the cooling effect of deforestation.

304

305 Table 2. Changes in key climate variables from regional and global deforestation
 306 experiments. “ Δ ” denotes change relative to the control experiment. The value for each
 307 climate variable is the area-weighted change over deforested areas for different latitude
 308 zones. The symbol “ \uparrow ” denotes upward and “ \downarrow ” denotes downward. Units are W/m^2 for
 309 energy flux, K for temperature, mm/day for precipitation, and unitless for albedo.

	Tropical (20°N-20°S)		Temperate (20°N-50°N)		Boreal (50°N-90°N)	
	Regional	Global	Regional	Global	Regional	Global
Temperature	2.22	2.06	-0.84	-1.56	-1.70	-2.42
Precipitation	-3.75	-3.89	-0.71	-0.89	-0.14	-0.21
ET	-82	-85	-17	-21	-5	-5
Sensible heat (ΔH)	15	13	-12	-13	-14	-14
Shortwave \downarrow ($\Delta SW\downarrow$)	50	53	18	21	13	14
Shortwave \uparrow ($\Delta SW\uparrow$)	88	95	41	48	37	38
Longwave \downarrow ($\Delta LW\downarrow$)	-14	-17	-11	-17	-6	-11
Net shortwave (ΔSW)	-38	-42	-23	-27	-24	-24

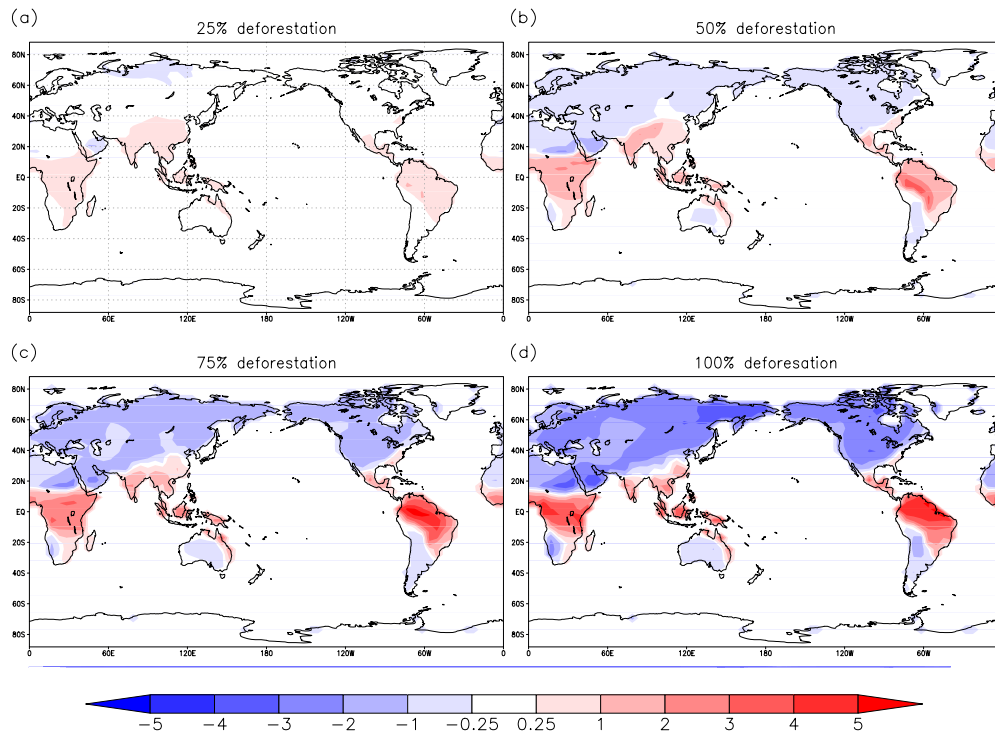
Albedo	0.26	0.28	0.17	0.18	0.22	0.22
Turbulent flux ($\Delta T_{ub} = \Delta H + \Delta ET$)	-67	-72	-29	-34	-19	-19
Available energy ($\Delta A_{va} = \Delta SW + LW\downarrow$)	-52	-59	-34	-44	-30	-35

310

311 **3.2 Sensitivity of temperature change to spatial extent and degree of**
312 **vegetation change**

313 The influence of spatial extent of deforestation can be clearly seen by comparing the
314 temperature response in a given region under regional and global deforestation
315 experiments. While similar in spatial pattern, temperature change in the global
316 deforestation experiment (Figure 1d) is much stronger than those in the regional
317 deforestation, especially in mid and high latitudes (Table 2). From the regional to global
318 scale, deforestation-induced cooling increases from -0.84K to -1.56K, and from -1.70K to
319 -2.42 K in the northern temperate and boreal regions, respectively. In contrast, warming
320 in the tropics is less affected and even slightly decreases from 2.22K in the regional
321 deforestation case to 2.06K in the global case. This is because global deforestation leads
322 to a stronger reduction of both absorbed shortwave radiation and downward longwave
323 radiation, both amplifying the cooling effects (Table 2) that reduce tropical warming and
324 enhance high-latitude cooling. Such dampened tropical warming and enhanced extra-
325 tropical cooling from regional to global deforestation experiments are supported by a
326 recent study (Devaraju *et al.*, 2015). Overall, an amplified temperature change in the
327 global deforestation experiment is expected as it generates a stronger perturbation in the
328 atmosphere, but the latitudinal temperature response is well preserved despite the
329 increase in the spatial extent of deforestation from regional to global.

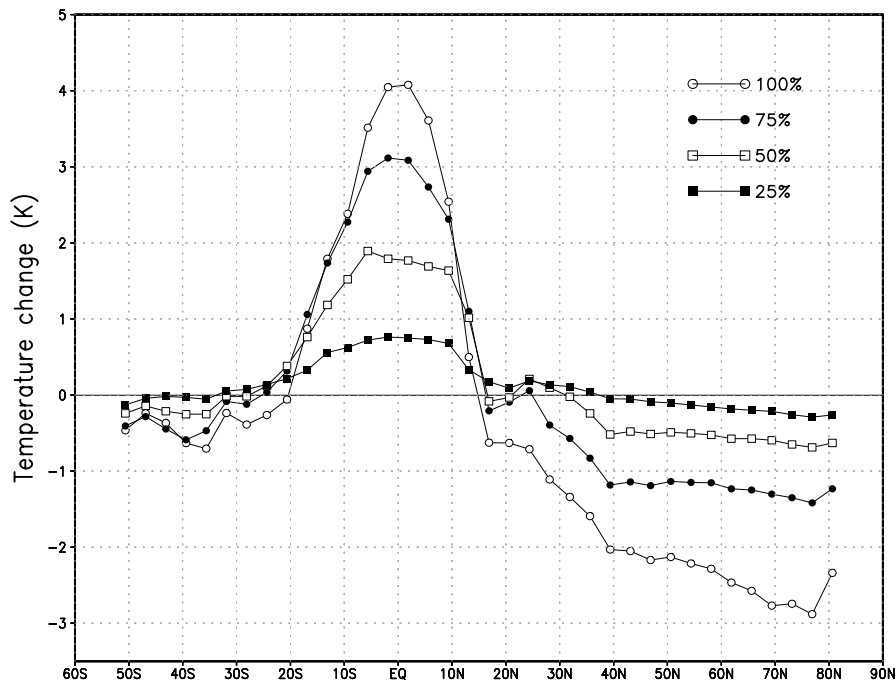
330 By looking at a set of experiments with varying deforestation fractions, we found
331 temperature change is also sensitive to degree of vegetation change (see Figure 2, Table
332 3). Deforestation fraction refers to the percentage of trees removed relative to the original
333 coverage (25%, 50%, 75%, and 100%), which is representative of the real areas that have
334 been deforested. For 25% deforestation fraction, temperature is virtually unaffected in
335 most areas except for a weak warming in the tropics. As forest-loss fraction goes up to
336 50%, a latitudinal temperature change emerges with discernible tropical warming and
337 weak cooling in mid and high latitudes (Figure 3). Higher deforestation fractions of 75%
338 and 100% result in a greater temperature change and a more prominent latitudinal pattern.
339 Generally, the magnitude of temperature change responds nonlinearly to increases of
340 deforestation fraction, with much larger changes at high deforestation fractions (Figure 3,
341 Table 3). This nonlinearity can either arise from the response of biophysical land
342 parameters to deforestation, or from the climate response (i.e., temperature response) to
343 biophysical changes. We found nonlinearities in both of these aspects (Figure S6).
344
345
346



347

Figure 2. Temperature change for global deforestation experiments with different deforestation fractions at (a) 25%, (b) 50%, (c) 75% and (d) 100%

348



349

Figure 3. Latitudinal pattern of temperature change with different deforestation fractions

350

351 Table 3. Changes in key climate variables from global deforestation with different
 352 deforestation fractions. “ Δ ” denotes change relative to the control experiment. The value
 353 for each climate variable is the area-weighted change over deforested areas for different
 354 latitude zones. The symbol “ \uparrow ” denotes upward and “ \downarrow ” denotes downward. Units are
 355 W/m^2 for energy flux, K for temperature, mm/day for precipitation, and unitless for
 356 albedo.

Region	Tropical (20°N-20°S)				Temperate (20°N-50°N)				Boreal (50°N-90°N)			
	25%	50%	75%	100%	25%	50%	75%	100%	25%	50%	75%	100%
Deforestation fraction												
Temperature	0.53	1.22	1.86	2.06	0.03	-0.23	-0.75	-1.56	-0.17	-0.55	-1.21	-2.42
Precipitation	-0.58	-1.54	-2.63	-3.89	-0.17	-0.49	-0.71	-0.89	-0.03	-0.07	-0.12	-0.21
ET	-15.3	-37.1	-59.2	-85.5	-4.6	-12.4	-17.4	-20.7	-0.6	-1.6	-2.6	-5.2
Sensible heat (ΔH)	12.0	23.2	27.8	13.3	2.4	0.9	-4.1	-13.3	-1.2	-3.6	-8.0	-14.1

Shortwave↓ ($\Delta SW \downarrow$)	3.8	13.1	27.1	52.6	1.7	7.7	14	21.3	1.4	3.9	7.7	13.8
Shortwave↑ ($\Delta SW \uparrow$)	3.0	16.1	40.5	94.9	2.6	14.8	29.7	48.3	3.5	9.8	20.2	37.8
Longwave↓ ($\Delta LW \downarrow$)	-0.7	-3.2	-6.7	-16.9	-1.2	-5.8	-10.6	-16.9	-0.8	-2.7	-5.6	-10.5
Δ Albedo	0.01	0.05	0.12	0.28	0.01	0.06	0.11	0.18	0.02	0.06	0.12	0.22

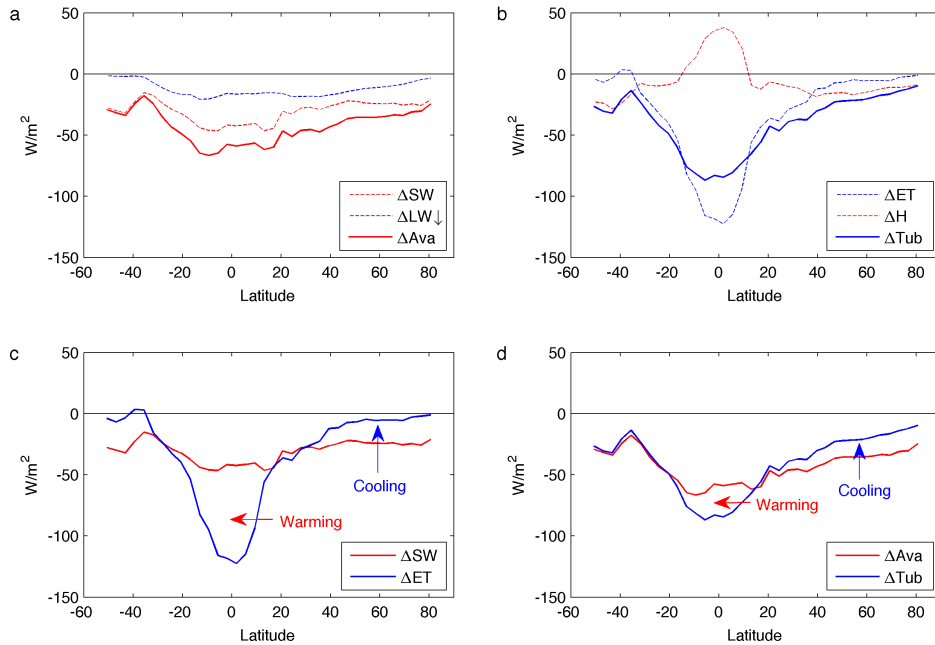
357 **3.3 Role of surface energy balance in latitudinal temperature change**

358 Temperature change is driven by altered surface energy balance in response to forest
359 removal. Among them, changes in shortwave radiation absorption (ΔSW) and
360 evapotranspiration (ΔET) can largely determine the sign and magnitude of temperature
361 response to deforestation. Deforestation can increase surface albedo, leading to reduced
362 absorbed shortwave radiation at the surface (ΔSW) which acts as a cooling mechanism,
363 while decreased ET (ΔET) can produce a warming effect due to weakened latent cooling.

364 Figure 4c shows the latitudinal pattern of ΔSW and ΔET . Although the largest
365 decreases are observed in the low latitudes and become smaller as latitude increases, the
366 relative importance of these two varies across latitudes as also reported in Davin & de
367 Noblet-Ducoudre (2010) and Li *et al.* (2015). In the tropics, ET declines (warming effect)
368 more than the absorbed shortwave radiation (cooling effect). This ΔET -dominated energy
369 imbalance is compensated by increase in temperature, outgoing longwave radiation, and
370 sensible heat. Beyond the tropics, the opposite occurs, as ET declines less than absorbed
371 shortwave radiation, therefore temperature and sensible heat decrease in response to the
372 ΔSW dominated energy imbalance. Specifically, mid latitude is a transition region where
373 ΔET and ΔSW in the south are relatively close to each other but in the north are quite
374 different. In high latitudes, ΔET is negligible whereas ΔSW maintains similar magnitude
375 as in the mid latitudes, thus resulting in the most significant temperature decrease.

376 Although ΔSW and ΔET determine the basic latitudinal pattern of temperature change,
377 changes in downward longwave radiation ($\Delta LW\downarrow$) and sensible heat (ΔH) also have
378 influence. While $\Delta SW\downarrow$ (changes in downward shortwave) could be considered as a part
379 of atmospheric feedback due to cloud cover change, we find that ΔSW is still dominated
380 by $\Delta SW\uparrow$ (changes in upward shortwave) due to albedo change (Figure S7). $\Delta LW\downarrow$
381 decreases across all latitudes due to less cloud cover, while sensible heat increases in the
382 tropics and decreases in other latitudes. $\Delta LW\downarrow$ is combined with ΔSW to give the
383 available energy ($\Delta A_{va} = \Delta SW + \Delta LW\downarrow$) and ΔH is combined with ΔET to give the
384 turbulence energy ($\Delta T_{ub} = \Delta ET + \Delta H$), corresponding to the changes in received and
385 dissipated energy, respectively. Available energy warms the land surface while
386 turbulence energy cools the surface (de Noblet-Ducoudré *et al.*, 2012). The difference of
387 these two is the outgoing longwave radiation, which is a function of ground temperature,
388 and is equivalent to ground temperature change. As shown in Figure 4d, the latitudinal
389 changes of the available and turbulence energy largely resemble that of ΔSW and ΔET ,
390 but with some noticeable differences. Comparing with ΔSW , reduction in available
391 energy (ΔA_{va}) is larger across all latitudes, suggesting an amplifying feedback
392 mechanism through $\Delta LW\downarrow$ due to reduced cloud cover (more reduction in $\Delta SW + \Delta LW\downarrow$,
393 Figure 4a). However, ΔT_{ub} is smaller than ΔET in the tropics (less reduction for
394 $\Delta ET + \Delta H$, Figure 4b) but larger than ΔET in the mid and high latitudes (more reduction
395 for $\Delta ET + \Delta H$, Figure 4b), showing that the warming signal can be either weakened or
396 enhanced when ΔH is considered (see Table 2). Overall, the latitude pattern of ΔSW and
397 ΔET in the southern hemisphere is influenced more by $\Delta LW\downarrow$ and ΔH than in the
398 northern hemisphere. In the southern hemisphere, the originally large energy difference

399 between ΔSW and ΔET disappears when $\Delta LW\downarrow$ and ΔH are accounted for, resulting in a
 400 dampened energy difference of ΔAve and ΔTub .



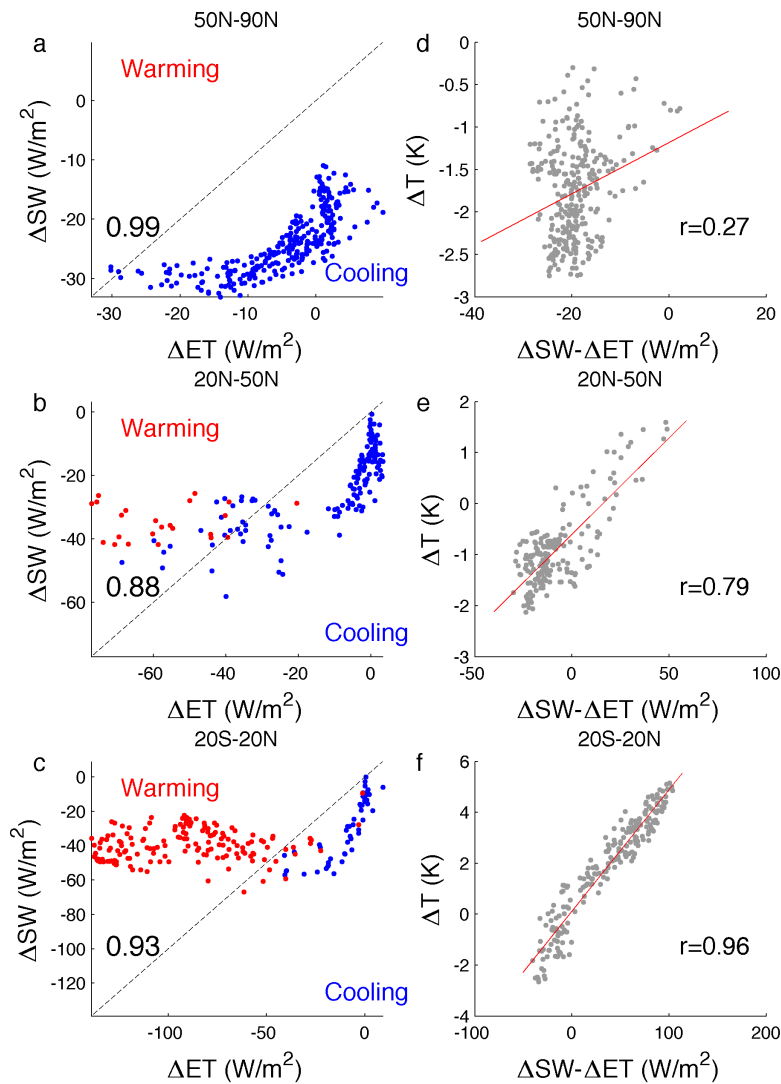
401

Figure 4. Latitudinal pattern of changes in surface energy balance. (a) Changes in absorbed shortwave radiation (ΔSW), downward longwave radiation ($\Delta LW\downarrow$), and available energy ($\Delta Ave = \Delta SW + \Delta LW\downarrow$). (b) Changes in evapotranspiration (ΔET), sensible heat (ΔH), and turbulence energy ($\Delta Tub = \Delta ET + \Delta H$). (c) ΔSW and ΔET . (d) ΔAve and ΔTub

402

403 Analysis above shows that the basic latitudinal pattern of ΔSW and ΔET can explain
 404 most of the latitudinal temperature response regardless of other changes and feedbacks
 405 (e.g., changes in downward longwave radiation and sensible heat). Here we evaluate the
 406 extent to which relative importance of ΔSW and ΔET can explain the spatially varying
 407 temperature change in terms of its sign and amplitude. The sign of temperature change

408 can be approximated by a simple ratio of $\Delta ET/\Delta SW$. The accuracy of this approximation
409 depends on the strength of the basic pattern imposed by ΔSW and ΔET against other
410 changes. A larger-than-one ratio suggests ΔET warming exceeds ΔSW cooling and
411 temperature is likely to increase, whereas a smaller-than-one ratio suggests ΔSW cooling
412 is stronger than ΔET warming and temperature tends to decrease. We used results from
413 the regional deforestation numerical experiments to demonstrate this feature. Figure 5
414 shows the deforested grid points in the model with their ΔET and ΔSW plotted on the x
415 and y axes, with colors representing the sign of temperature change. Deforested points
416 with increased temperature (red) are often located in the upper-left space of the $\Delta ET =$
417 ΔSW line where warming is anticipated ($\Delta ET > \Delta SW$), while points with decreased
418 temperature fall into the lower-right space where cooling is anticipated ($\Delta ET < \Delta SW$). It
419 turns out that ΔET and ΔSW alone can explain 93%, 88%, and 99% of deforested points
420 for the direction of temperature change in the tropical, temperate, and boreal regions,
421 respectively. In addition, there is tendency towards smaller $\Delta ET/\Delta SW$ ratios at higher
422 latitudes and drier areas in the global deforestation experiment (Figure S8), suggesting a
423 decreasing importance of ΔET over ΔSW . Few exceptions exist because longwave and
424 sensible heat changes may also influence temperature change but are not considered here.
425 Furthermore, the amplitude of temperature change is related to the difference of ΔSW and
426 ΔET . As shown in Figure 5d-f, $\Delta SW - \Delta ET$ is highly correlated with the amplitude of
427 temperature change in the tropical ($r=0.96$) and temperate regions ($r=0.79$), but not in the
428 boreal region ($r=0.27$).



429

Figure 5. Changes in ET (ΔET), absorbed shortwave radiation (ΔSW) and their relationship with temperature change (ΔT) over deforestation areas. (a-c) Deforested points with their ΔSW , ΔET , and the sign of ΔT . The upper left area means ET warming exceeds albedo cooling; the lower right area means albedo cooling exceeds ET warming. Blue (red) are the actual grid points where temperature decreased (increased). Number denotes the percentage of deforested points whose sign of ΔT agrees with anticipation of

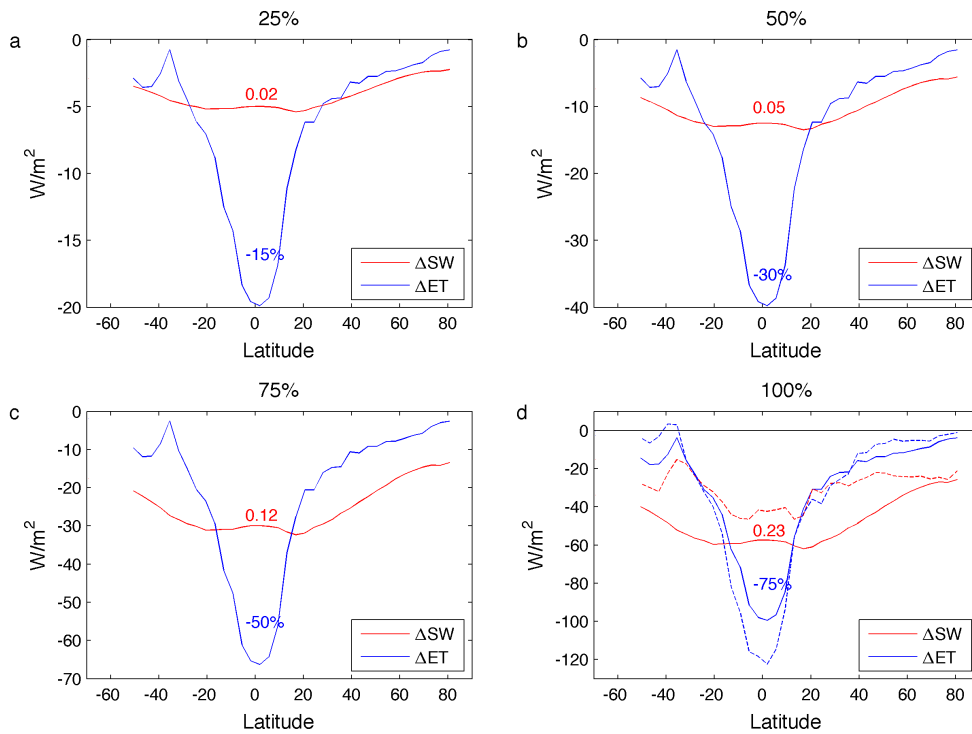
ΔSW and ΔET . (d-f) Spatial relationship between ΔSW - ΔET and the amplitude of ΔT . Red line is the regression line, and r is the correlation coefficient. (a,d) Boreal deforestation; (b,e) North temperate deforestation; (c,f) Tropical deforestation.

430 **3.4 Influence of background climate on surface energy change and** 431 **temperature change**

432 The latitude-dependent pattern for ΔSW and ΔET could arise from the intrinsic
433 latitudinal distribution in background climate, e.g., solar radiation and precipitation/ET
434 decrease with latitude increase. Therefore, the same amount of albedo change would
435 translate into a larger ΔSW in lower latitudes due to the geographic distribution of solar
436 radiation. Likewise, given the same ET reduction rate, a larger ΔET is expected in the
437 tropics than in high latitudes.

438 The influence of background climate can be illustrated by a simple calculation.
439 Assume that deforestation causes albedo increase by 0.02, 0.05, 0.12, and 0.23 uniformly
440 across all latitudes and ET decrease by 15%, 30%, 50%, and 75% compared to their
441 baseline climatology, respectively. Multiplying these change rates by the baseline
442 shortwave radiation and ET, we obtain the corresponding ΔSW and ΔET without
443 considering any climate feedback. For demonstration purpose, the change rates chosen
444 here for albedo and ET roughly correspond to the global averaged changes in the four
445 deforestation fraction experiments (deforestation fraction ranges from 25% to 100%, see
446 group II experiment). Interestingly, the calculated ΔSW and ΔET (Figure 6) agree well
447 with the simulation (Figure 4c). The main features, including $\Delta ET > \Delta SW$ in the tropics
448 and $\Delta ET < \Delta SW$ in the extratropics, are captured. We also used the satellite derived ET
449 and shortwave radiation data from Li *et al.* (2015) to perform the calculation (see Figure

450 S9). The results generally support the findings from Figure 6, except for the two
451 combinations with small changes in albedo and ET. For these two cases, the anticipated
452 pattern is not captured mainly because of the chosen low albedo change in high latitude,
453 which leads to an underestimation of ΔSW . It should be emphasized that the albedo and
454 ET change rates in reality have more complicated patterns than what we assume in the
455 calculation. Nevertheless, our simple calculation still reveals the role of the baseline
456 climate in shaping the latitude-dependent temperature change to deforestation.
457



458

Figure 6. The latitudinal pattern of ΔSW and ΔET calculated by multiplying their background climate values with different rates for albedo (red number, from 0.02 in (a) to 0.23 in (d)) and ET changes (blue number, from -15% in (a) to -75% in (d)). In (d),

dashed lines are simulated changes from global deforestation for comparison with the calculated changes (solid line).

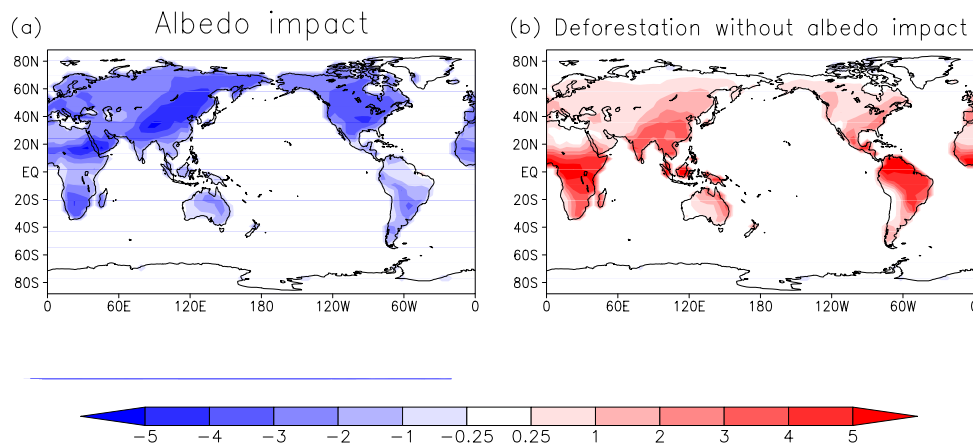
459 Further evidence comes from the spatial relationship between background climate and
460 temperature response to deforestation. We found baseline precipitation is highly
461 correlated with ΔET ($r=-0.98$) and with ΔT ($r=0.87$), suggesting that precipitation can
462 influence temperature change by controlling ET change. This is also supported by the
463 ratio of $\Delta ET/\Delta SW$ in Figure S8 where larger ΔET over ΔSW is found in wetter areas, and
464 by observations from air temperature (Zhang *et al.*, 2014) and physical mechanisms
465 pertaining to soil moisture (Swann *et al.*, 2012). Therefore, spatial variation of
466 temperature change is partly due to background climate. For instance, temperature
467 decreases in the tropical deforested areas like Sahel, west Amazon, and southwestern
468 Africa, because dry climate limits ΔET , thus temperature change is dominated by the
469 cooling effect from ΔSW . In contrast, in wet temperate deforested areas like South China,
470 India, and parts of North America, temperature increases because of the dominant
471 warming effect from ΔET .

472 **3.5 Contribution of individual biophysical processes to the latitudinal** 473 **temperature change**

474 The aforementioned changes in temperature and surface energy balance are triggered
475 by the altered biophysical variables such as albedo, roughness, ET efficiency, etc. as a
476 result of deforestation. The effect of each individual biophysical factor and its
477 contribution to temperature change are evaluated in this section.

478 (1) Albedo

479 The impact of albedo change can be isolated by the difference of ALL – noALB (see
480 Method Section), as shown in Figure 7a. As expected, albedo change causes significant
481 temperature decrease over all affected regions. Surprisingly, the strongest cooling appears
482 in the northern temperate region instead of the tropics where the largest albedo increase
483 occurs (Table 4). This indicates the strength of perturbation is not the only factor for
484 determining spatially varying temperature change. The magnitude of cooling in the boreal
485 region is similar to the temperate region, because of no amplified albedo change due to
486 snow. If deforestation did not change albedo, there would be a substantial warming over
487 all affected regions (noALB – CTL, Figure 7b), accompanied with decreased ET and
488 very little change in absorbed shortwave radiation (SW). This is expected because the
489 warming effect of ΔET dominates temperature change when albedo effect is absent.
490



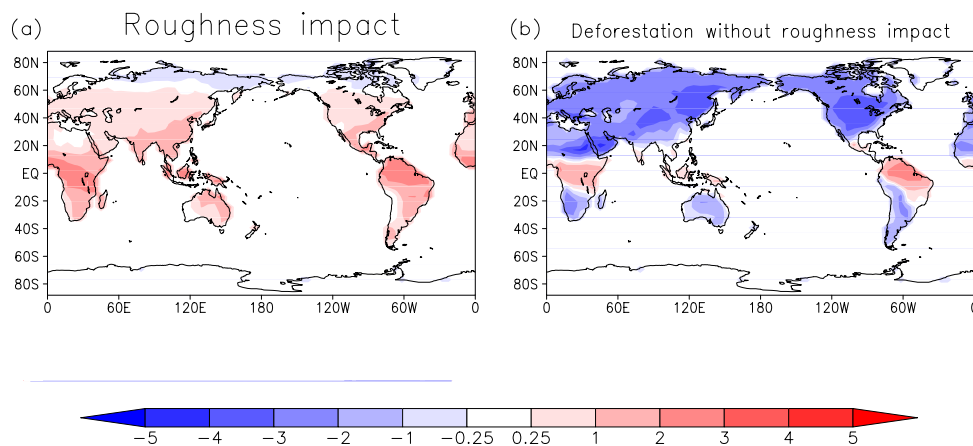
491

Figure 7. (a) Impact of Albedo (only) on temperature change (b) temperature change without albedo impact (K)

492

493 (2) Roughness

494 Roughness can affect turbulence (ET as well as sensible heat) flux between land
495 surface and atmosphere. Higher roughness facilitates absorbed shortwave energy to be
496 dissipated as turbulence, while smaller roughness suppresses this process and could have
497 a warming effect. Effect of roughness on climate can be isolated by the difference All –
498 noRGH. Roughness change as well as its impact are more pronounced in the tropical
499 region (Table 4). As is seen in Figure 8a, reduced roughness warms most areas except for
500 the upper northern latitudes, with warming decreasing from the tropics to high latitudes;
501 see also Davin & de Noblet-Ducoudre (2010). Without roughness change, deforestation
502 would cause less warming (Figure 8b) and less reduction in turbulence energy (not shown)
503 than regular deforestation. Moreover, Figure 8b also shows the combined effects from
504 albedo and evapotranspiration efficiency since roughness effect is excluded. Thus, the
505 existence of a tropical warming in some regions implies that the reduction in
506 evapotranspiration efficiency remains dominant and outweighs the albedo impact in this
507 situation.



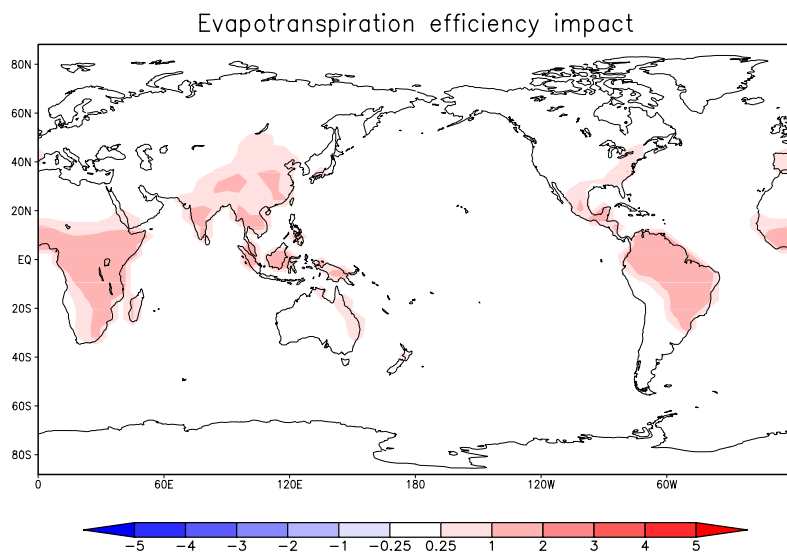
508

Figure 8. (a) Impact of roughness (only) on temperature (K); (b) temperature change without roughness

509

510 (3) Evapotranspiration efficiency

511 Evapotranspiration efficiency refers to the ability of partitioning available energy into
512 evapotranspiration more than into sensible heat. The conversion of forest to bare land
513 favors more turbulence energy to be transferred in the form of sensible heat rather than
514 ET, resulting in higher Bowen ratio. The impact of altered ET efficiency can be separated
515 by EVA – CTL, showing a noticeable warming in the tropical regions and some parts of
516 the temperate region, and negligible impact in high latitude (Figure 9). It seems that
517 changed ET efficiency has a significant impact only over regions with wet climate, which
518 may be due to the close coupling between precipitation and ET change.



519

Figure 9. Evapotranspiration efficiency impact on temperature change (K)

520

521 Table 4. Summary of influence of individual biophysical factors on temperature change.
 522 Numbers in parentheses are changes in albedo and roughness. Albedo is unitless and unit
 523 for roughness is m.

524

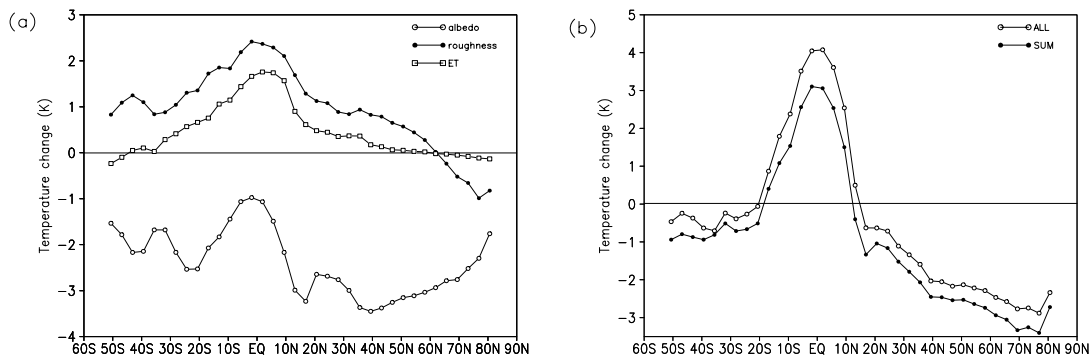
	Global (ALL – CTL)	Albedo (ALL – noALB)	Roughness (ALL-noRGH)	Evapotranspiration efficiency (EVA – CTL)
50°N-90°N	-2.42	-2.93 (0.22)	0.05 (0.86)	0
20°N-50°N	-1.56	-3.1 (0.18)	0.86 (0.66)	0.27
20°S-20°N	2.06	-1.92 (0.28)	1.92 (1.33)	1.22

525 ALL: global deforestation; noALB: global deforestation without albedo change; noRGH:
 526 global deforestation without roughness change; EVA: global deforestation without both
 527 albedo and roughness change.

528

529 By summing up the contributions from individual biophysical factors linearly (ALL –
 530 noALB + ALL – noRGH + EVA – CTL), we reconstruct temperature change, which
 531 closely agrees with the actual signal (ALL – CTL) in terms of both latitudinal (Figure 10)
 532 and geographical patterns (Figure 11). Latitudinal features are inherited in the
 533 contribution of each individual component (Table 4). Albedo effect generally increases
 534 with latitude whereas roughness and evapotranspiration efficiency effects decrease with
 535 latitude. Therefore, the largest temperature increase in the tropical region (2.06K)
 536 originates from the warming effect of changed roughness (1.92K) and evapotranspiration
 537 efficiency (1.22K), and is counteracted by a comparatively small albedo cooling (-1.92K).
 538 In the extratropics, temperature response is dominated by albedo cooling, with similar
 539 strengths in the northern temperate (-3.01K) and boreal (-2.93K) regions. But such
 540 cooling is partially canceled by the weaker warming effect of roughness (0.86K) and
 541 evapotranspiration efficiency (0.27K) in the temperate region and no compensation at all

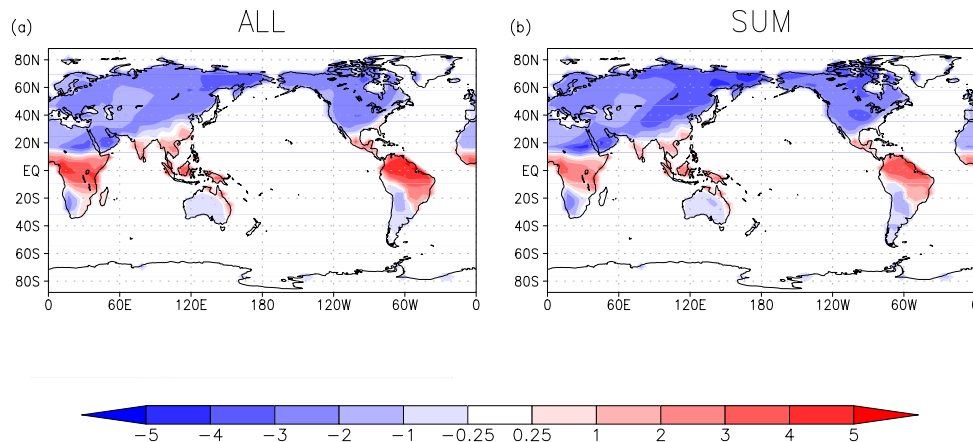
542 in the boreal region. The latitudinal pattern caused by each biophysical factor is less
 543 likely to be due to the latitudinal signal from biophysical change per se, because
 544 biophysical change does not match the latitude pattern of temperature response. For
 545 example, the largest temperature change does not occur where the largest biophysical
 546 change (e.g., albedo and roughness) occurs. This shows the complex interactions in the
 547 translation from the initial perturbation to subsequent climate response, which varies by
 548 latitude. Biophysical impacts are strongly regulated by the baseline climate where
 549 vegetation change occurs, as also demonstrated in Pitman *et al.* (2011).
 550



551

Figure 10. (a) Latitudinal patterns of the contribution of individual biophysical factors to temperature change and (b) reconstructed temperature change from individual biophysical effects (SUM=ALL – noALB + ALL – noRGH + EVA – CTL)

552



553

Figure 11. Spatial patterns of (a) actual temperature change and (b) reconstructed temperature change ($SUM=ALL - noALB + ALL - noRGH + EVA - CTL$)

554 **4. Discussion**

555 Our results show patterns of temperature change as a result of deforestation that are in
 556 line with the conclusions of previous modeling studies, e.g., strong tropical warming
 557 (Nobre *et al.*, 1991; Snyder *et al.*, 2004), moderate temperate cooling, and strong boreal
 558 cooling (Bonan *et al.*, 1992, 1995; Betts, 2000), but few of them consider the spatial scale
 559 of deforestation. We found that temperature change varies nonlinearly with both the
 560 spatial scale and the fraction of forest removed, with increasingly larger temperature
 561 change as disturbance grows, but the overall latitudinal pattern is not altered. This scale-
 562 dependent relationship between temperature change and deforestation reflects a
 563 perturbation-response relationship derived from the existing mechanisms of the model in
 564 which non-linearity is found. However, it does not exactly emulate the influence of
 565 physical processes operating at various scales in the real world, because many scale-
 566 related processes cannot be fully resolved in a model with a fixed complexity. For

567 example, many meso-scale processes cannot be included in a global model. This makes it
568 difficult to compare our results to observational study results that span different spatial
569 scales.

570 We found that changes in shortwave radiation absorption (ΔSW) and
571 evapotranspiration (ΔET) can largely determine the sign and amplitude of temperature
572 change, as well as its latitudinal and spatial patterns in response to deforestation. In a
573 global deforestation scenario, more than 90% of the sign of temperature change over
574 deforested areas can be explained by ΔSW and ΔET . Although ΔET and ΔSW can be
575 influenced by other factors and feedbacks, they still provide useful diagnostic information
576 for temperature change and serve as a first order approximation. Using this information,
577 albedo and ET changes (two variables readily available from satellite data) can be
578 potentially applied to evaluate the possible impact of undergoing land cover change on
579 local and regional temperature (Loarie *et al.*, 2011; Peng *et al.*, 2014; Li *et al.*, 2015).

580 To a large extent, the latitude-dependent temperature response to deforestation and its
581 spatial variability can be attributed to background climate condition, such as solar
582 radiation, precipitation, and snow, which in turn affect the biophysical impact of
583 vegetation change. Further evidence comes from the contribution of each biophysical
584 factor, i.e., albedo, roughness, and ET efficiency, on the temperature response. Although
585 these factors drive temperature change in different directions, their contributions also
586 have clear latitudinal patterns (Davin & de Noblet-Ducoudre, 2010). This indicates that
587 climate condition manifests its influence either explicitly in the temperature response
588 through controlling changes on surface energy balance, or implicitly in the magnitude of
589 biophysical alteration triggered by deforestation. After careful analysis of our model, our

590 results show that the latitudinal pattern of temperature change is due to the explicit
591 impact of climate condition.

592 We acknowledge certain limitations and important issues that are not fully addressed
593 in this study. Previous studies showed an important role of oceanic feedback which could
594 cause additional cooling through albedo change (e.g., sea-ice albedo feedback) and could
595 override temperature change over land in mid latitudes (Claussen *et al.*, 2001; Davin &
596 de Noblet-Ducoudré, 2010), but our ocean model is not interactive so such dynamics
597 could not be studied here. In the simulation, we used the SST climatology of 1960-1990
598 with seasonal cycle only that can minimize inter-annual variability and therefore amplify
599 the strength of deforestation signal to climate variability in terms of statistical
600 significance. If a different period of the SST climatology had been used, the simulated
601 climate may have been slightly different including differences in vegetation distribution
602 and deforestation impacts. Nevertheless, our results are unlikely to be substantially
603 changed by the choice of SST climatology, because a background climate change as large
604 as that coming from $1\times\text{CO}_2$ (280 ppm) increased to $2\times\text{CO}_2$ (280 ppm) can only modify
605 the climate impact over certain transitional regions (Pitman *et al.*, 2011).

606 Furthermore, in this study we use ground temperature as the variable for accessing the
607 deforestation impact. In other studies, and perhaps more commonly, this component
608 could be analyzed using air temperature, although research based on ground temperature
609 (McGuffie *et al.*, 1995; Kendra Gotangco Castillo & Gurney, 2012) or surface
610 temperature (Davin & de Noblet-Ducoudré, 2010) is also seen in the literature. Although
611 these two have been shown to often agree with one another at larger scales (Jin *et al.*,
612 1997), it is worth investigating whether they have different responses to vegetation

613 change (Baldocchi & Ma, 2013; Zhao & Jackson, 2014; Li *et al.*, 2015). Moreover, the
614 response of maximum and minimum temperatures also differ from the daily averaged
615 temperature (Zhang *et al.*, 2014; Li *et al.*, 2015), a problem that has received less
616 attention in modeling studies.

617 Finally, results from a single model are subject to uncertainty and some features might
618 be model-dependent. For instance, some biases in the simulated climate of the model may
619 lead to shifts in vegetation distribution and thus could influence the deforestation impact.
620 To combat this, model inter-comparison projects like Land-Use and Climate,
621 Identification of Robust Impacts (LUCID) experiments (Pitman *et al.*, 2009) can help to
622 distinguish robust findings against model uncertainty. The participant models in LUCID
623 show consistency in how land cover change affects available energy but diverge greatly
624 on energy partition between latent and sensible heat flux changes (de Noblet-Ducoudré *et*
625 *al.*, 2012), indicating large uncertainty lies in the response of non-radiative process to
626 land cover change, especially for ET (Boisier *et al.*, 2012). Therefore, considerable effort
627 is required to improve model performance in the simulation of land processes, and new
628 inter-comparison projects such as LUMIP (Land Use Model Intercomparison Project,
629 <https://cmip.ucar.edu/lumip>) are highly valuable. In addition, observational studies are
630 indispensable as they can offer new insights and serve as a reference benchmark for
631 model results, especially those using new techniques and datasets such as satellite data.

632

633 **Author contributions:**

634 Y. Li designed and carried out the experiments; Y. Li and N. De Noblet-Ducoudré
635 analyzed the data; all authors contributed to the discussion and writing of the paper.

636

Acknowledgements

637 This work is supported by the National Basic Research Program of China (Grant No.
638 2015CB4527022), the National Natural Science Foundation of China (Grant No.
639 41130534 and 41371096), and the Maryland Council on the Environment. Y. Li also
640 received support from the China Scholar Council (Fellowship No. 201306010169).
641 S. Motesharrei received support from the National Socio-Environmental Synthesis Center
642 (SESYNC) —NSF award DBI-1052875. We thank Andy Pitman for his constructive and
643 insightful comments on this paper. Y. Li thanks Fang Zhao for his help with the model
644 simulations. We thank Laura Bracaglia for careful reading of the manuscript and helpful
645 edits on the writing.

646

References:

- 647 Allen CD, Macalady AK, Chenchouni H et al. (2010) A global overview of drought and
648 heat-induced tree mortality reveals emerging climate change risks for forests. *Forest
649 Ecology and Management*, **259**, 660–684.
- 650 Avissar R, Silva Dias PL, Sivla Dias MAF, Nobre C (2002) The Large-Scale Biosphere-
651 Atmosphere Experiment in Amazonia (LBA): Insights and future research needs.
652 *Journal of Geophysical Research*, **107**, 1–6.
- 653 Baidya Roy S, Avissar R (2002) Impact of land use/land cover change on regional
654 hydrometeorology in Amazonia. *Journal of Geophysical Research*, **107**.
- 655 Bala G, Caldeira K, Wickett M, Phillips TJ, Lobell DB, Delire C, Mirin A (2007)

656 Combined climate and carbon-cycle effects of large-scale deforestation.
657 *Proceedings of the National Academy of Sciences of the United States of America*,
658 **104**, 6550–6555.

659 Baldocchi D, Ma S (2013) How will land use affect air temperature in the surface
660 boundary layer? Lessons learned from a comparative study on the energy balance of
661 an oak savanna and annual grassland. *Tellus B*, **1**, 1–19.

662 Betts RA (2000) Offset of the potential carbon sink from boreal forestation by decreases
663 in surface albedo. *Nature*, **408**, 187–190.

664 Betts RA, Falloon PD, Goldewijk KK, Ramankutty N (2007) Biogeophysical effects of
665 land use on climate: Model simulations of radiative forcing and large-scale
666 temperature change. *Agricultural and Forest Meteorology*, **142**, 216–233.

667 Boisier JP, de Noblet-Ducoudré N, Pitman a. J et al. (2012) Attributing the impacts of
668 land-cover changes in temperate regions on surface temperature and heat fluxes to
669 specific causes: Results from the first LUCID set of simulations. *Journal of*
670 *Geophysical Research: Atmospheres*, **117**, D12116.

671 Bonan GB (2008) Forests and climate change: Forcings, feedbacks, and the climate
672 benefits of forests. *Science*, **320**, 1444–1449.

673 Bonan GB, Pollard D, Thompson SL (1992) Effects of Boreal Forest Vegetation on
674 Global Climate. *Nature*, **359**, 716–718.

675 Bonan GB, Chapin FS, Thompson SL (1995) Boreal Forest and Tundra Ecosystems as

676 Components of the Climate System. *Climatic Change*, **29**, 145–167.

677 Bounoua L, DeFries R, Collatz GJ, Sellers P, Khan H (2002) Effects of land cover
678 conversion on surface climate. *Climatic Change*, **52**, 29–64.

679 Claussen M, Brovkin V, Ganopolski A (2001) Biogeophysical versus biogeochemical
680 feedbacks of large-scale land cover change. *Geophysical Research Letters*, **28**,
681 1011–1014.

682 Darnell WL, Staylor WF, Gupta SK, Ritchey NA, Wilber AC (1992) Seasonal variation
683 of surface radiation budget derived from International Satellite Cloud Climatology
684 Project C1 data. *Journal of Geophysical Research: Atmospheres*, **97**, 15741–15760.

685 Davin EL, de Noblet-Ducoudré N (2010) Climatic Impact of Global-Scale Deforestation:
686 Radiative versus Nonradiative Processes. *Journal of Climate*, **23**, 97–112.

687 Devaraju N, Bala G, Modak A (2015) Effects of large-scale deforestation on precipitation
688 in the monsoon regions: Remote versus local effects. *Proceedings of the National
689 Academy of Sciences*, **112**, 3257–3236.

690 Friedlingstein P, Cox P, Betts R et al. (2006) Climate–Carbon Cycle Feedback Analysis:
691 Results from the C4MIP Model Intercomparison. *Journal of Climate*, **19**, 3337–
692 3353.

693 Gibbard S, Caldeira K, Bala G, Phillips TJ, Wickett M (2005) Climate effects of global
694 land cover change. *Geophysical Research Letters*, **32**, L23705.

695 Hales K, Neelin JD, Zeng N (2004) Sensitivity of Tropical Land Climate to Leaf Area
696 Index: Role of Surface Conductance versus Albedo. *Journal of Climate*, **17**, 1459–
697 1473.

698 Hansen M, Potapov P, Moore R (2013) High-resolution global maps of 21st-century
699 forest cover change. *Science*, **850**, 850–853.

700 Jin M, Dickinson R, Vogelmann A (1997) A comparison of CCM2-BATS skin
701 temperature and surface-air temperature with satellite and surface observations.
702 *Journal of Climate*, **10**, 1505–1524.

703 Juang JY, Katul G, Siqueira M, Stoy P, Novick K (2007) Separating the effects of albedo
704 from eco-physiological changes on surface temperature along a successional
705 chronosequence in the southeastern United States. *Geophysical Research Letters*, **34**,
706 L21408.

707 Kendra Gotangco Castillo C, Gurney KR (2012) Exploring surface biophysical-climate
708 sensitivity to tropical deforestation rates using a GCM: A feasibility study. *Earth*
709 *Interactions*, **16**, 1–23.

710 Lean J, Rowntree P (1997) Understanding the sensitivity of a GCM simulation of
711 Amazonian deforestation to the specification of vegetation and soil characteristics.
712 *Journal of Climate*, **10**, 1216–1235.

713 Lee X, Goulden ML, Hollinger DY et al. (2011) Observed increase in local cooling effect
714 of deforestation at higher latitudes. *Nature*, **479**, 384–387.

715 Li Y, Zhao M, Motesharrei S, Mu Q, Kalnay E, Li S (2015) Local cooling and warming
716 effects of forest based on satellite data. *Nature communications*, **6:6603**.

717 Loarie SR, Lobell DB, Asner GP, Mu Q, Field CB (2011) Direct impacts on local climate
718 of sugar-cane expansion in Brazil. *Nature Climate Change*, **1**, 105–109.

719 Longobardi P, Montenegro A, Beltrami H, Eby M (2012) Spatial scale dependency of the
720 modelled climatic response to deforestation. *Biogeosciences Discussions*, **9**, 14639–
721 14687.

722 Maynard K, Royer J-F (2004) Sensitivity of a general circulation model to land surface
723 parameters in African tropical deforestation experiments. *Climate Dynamics*, **22**,
724 555–572.

725 McGuffie K, Henderson-Sellers A, Zhang H, Durbidge TB, Pitman AJ (1995) Global
726 climate sensitivity to tropical deforestation. *Global and Planetary Change*, **10**, 97–
727 128.

728 Neelin JD, Zeng N (2000) A Quasi-Equilibrium Tropical Circulation Model—
729 Formulation. *Journal of the Atmospheric Sciences*, **57**, 1741–1766.

730 de Noblet-Ducoudré N, Boisier J-P, Pitman A et al. (2012) Determining Robust Impacts
731 of Land-Use-Induced Land Cover Changes on Surface Climate over North America
732 and Eurasia: Results from the First Set of LUCID Experiments. *Journal of Climate*,
733 **25**, 3261–3281.

734 Nobre C, Sellers P, Shukla J (1991) Amazonian Deforestation and Regional Climate

735 Change. *Journal of Climate*, **4**, 957–998.

736 Peng S-S, Piao S, Zeng Z et al. (2014) Afforestation in China cools local land surface
737 temperature. *Proceedings of the National Academy of Sciences of the United States*
738 *of America*, **111**, 2915–2919.

739 Pitman AJ, de Noblet-Ducoudré N, Cruz FT et al. (2009) Uncertainties in climate
740 responses to past land cover change: First results from the LUCID intercomparison
741 study. *Geophysical Research Letters*, **36**, L14814.

742 Pitman AJ, Avila FB, Abramowitz G, Wang YP, Phipps SJ, de Noblet-Ducoudré N (2011)
743 Importance of background climate in determining impact of land-cover change on
744 regional climate. *Nature Climate Change*, **1**, 472–475.

745 Pitman AJ, Arneth A, Ganzeveld L (2012) Regionalizing global climate models.
746 *International Journal of Climatology*, **32**, 321–337.

747 Rayner N a., Brohan P, Parker DE et al. (2006) Improved analyses of changes and
748 uncertainties in sea surface temperature measured in Situ since the mid-nineteenth
749 century: The HadSST2 dataset. *Journal of Climate*, **19**, 446–469.

750 Runyan C (2012) Physical and biological feedbacks of deforestation. *Reviews of*
751 *Geophysics*, **50**, 1–32.

752 Sampaio G, Nobre C, Costa MH, Satyamurty P, Soares-Filho BS, Cardoso M (2007)
753 Regional climate change over eastern Amazonia caused by pasture and soybean
754 cropland expansion. *Geophysical Research Letters*, **34**, L17709.

- 755 Snyder PK (2010) The Influence of Tropical Deforestation on the Northern Hemisphere
756 Climate by Atmospheric Teleconnections. *Earth Interactions*, **14**, 1–34.
- 757 Snyder PK, Delire C, Foley JA (2004) Evaluating the influence of different vegetation
758 biomes on the global climate. *Climate Dynamics*, **23**, 279–302.
- 759 Souza DC, Oyama MD (2010) Climatic consequences of gradual desertification in the
760 semi-arid area of Northeast Brazil. *Theoretical and Applied Climatology*, **103**, 345–
761 357.
- 762 Swann ALS, Fung IY, Chiang JCH (2012) Mid-latitude afforestation shifts general
763 circulation and tropical precipitation. *Proceedings of the National Academy of
764 Sciences of the United States of America*, **109**, 712–6.
- 765 Wickham JD, Wade TG, Riitters KH (2013) Empirical analysis of the influence of forest
766 extent on annual and seasonal surface temperatures for the continental United States
767 (ed Peñuelas J). *Global Ecology and Biogeography*, **22**, 620–629.
- 768 Zeng N (2003) Glacial-interglacial atmospheric CO₂ change —The glacial burial
769 hypothesis. *Advances in Atmospheric Sciences*, **20**, 677–693.
- 770 Zeng N (2004) How strong is carbon cycle-climate feedback under global warming?
771 *Geophysical Research Letters*, **31**, L20203.
- 772 Zeng N, Neelin JD (2000) The Role of Vegetation Climate Interaction and Interannual
773 Variability in Shaping the African Savanna. *J. Climate*, **13**, 2665–2670.

- 774 Zeng N, Yoon J (2009) Expansion of the world's deserts due to vegetation-albedo
775 feedback under global warming. *Geophysical Research Letters*, **36**, L17401.
- 776 Zeng N, Neelin JD, Lau KM, Tucker CJ (1999) Enhancement of Interdecadal Climate
777 Variability in the Sahel by Vegetation Interaction. *Science*, **286**, 1537–1540.
- 778 Zeng N, Neelin JD, Chou C (2000) A Quasi-Equilibrium Tropical Circulation Model—
779 Implementation and Simulation. *Journal of the Atmospheric Sciences*, **57**, 1767–
780 1796.
- 781 Zeng N, Mariotti A, Wetzell P (2005) Terrestrial mechanisms of interannual CO₂
782 variability. *Global Biogeochemical Cycles*, **19**, 1–15.
- 783 Zhang M, Lee X, Yu G et al. (2014) Response of surface air temperature to small-scale
784 land clearing across latitudes. *Environmental Research Letters*, **9**, 034002.
- 785 Zhao K, Jackson R (2014) Biophysical forcings of land-use changes from potential
786 forestry activities in North America. *Ecological Monographs*, **84**, 329–353.

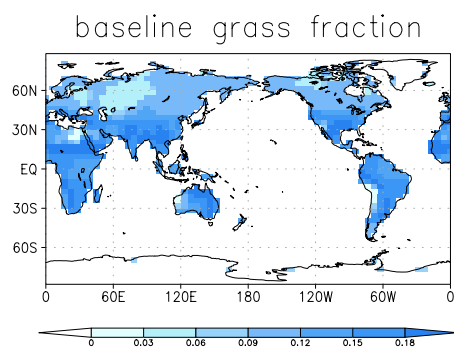
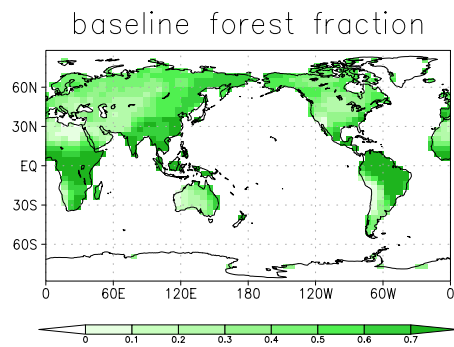
787

788 **Supplementary figures:**

789

790

791



792

793

Figure S1. Simulated vegetation distribution in the control experiment (CTL)

794

795

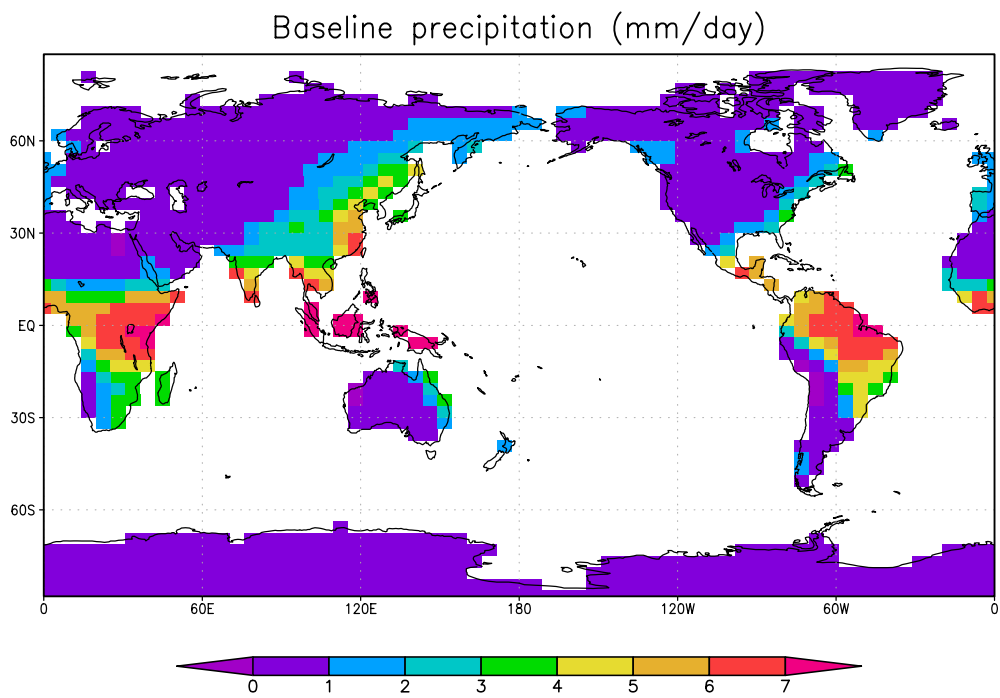
796

797

798

799

800



801

Figure S2. Annual mean precipitation simulated in the control experiment

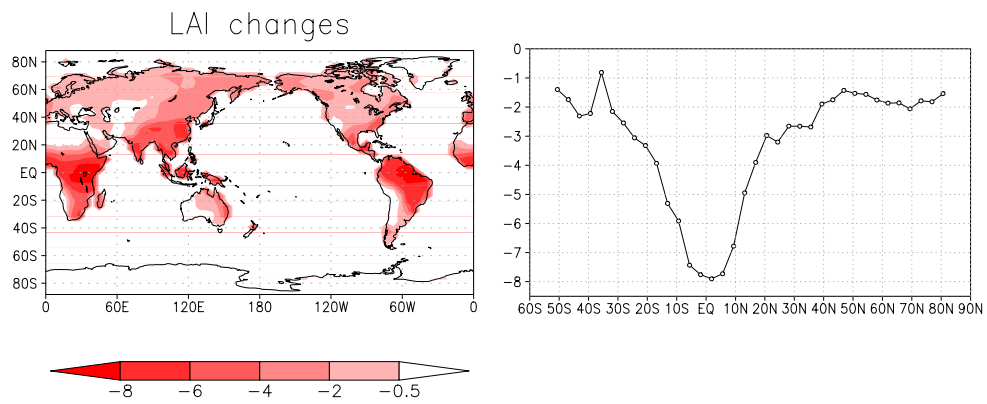


Figure S3. Spatial (left) and latitudinal (right) patterns of LAI changes due to global deforestation (Unit: m^2/m^2)

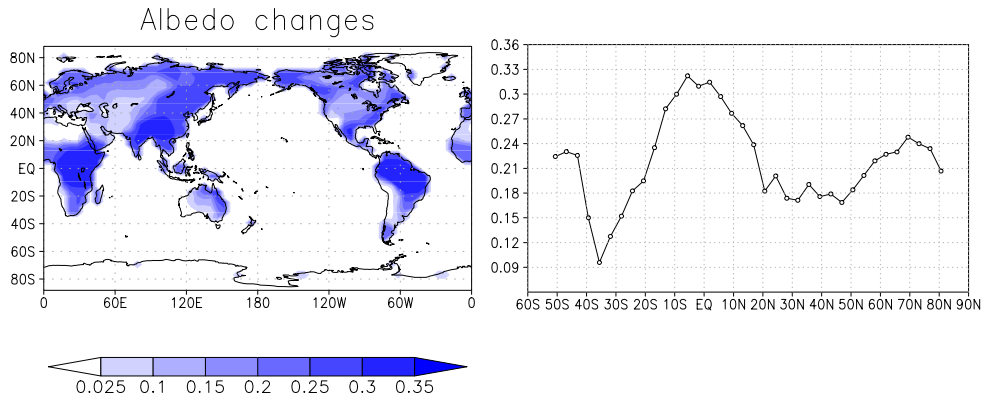


Figure S4. Spatial (left) and latitudinal (right) patterns of albedo changes due to global deforestation

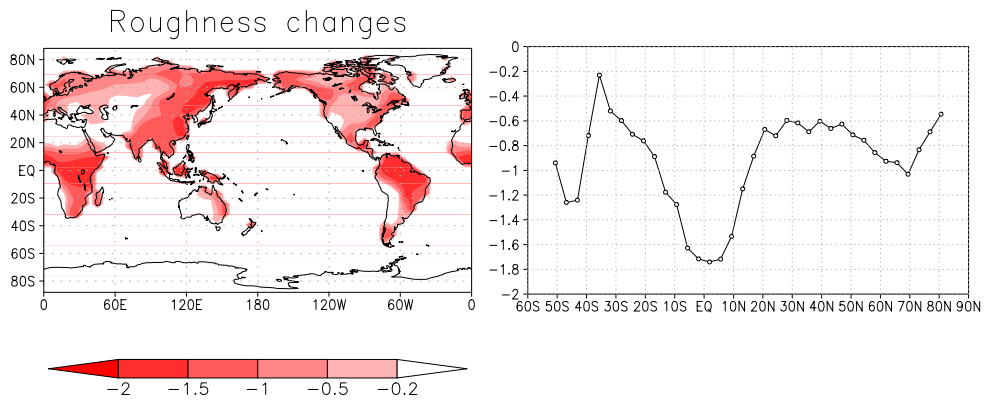


Figure S5. Spatial (left) and latitudinal (right) patterns of roughness changes due to global deforestation (Unit: m)

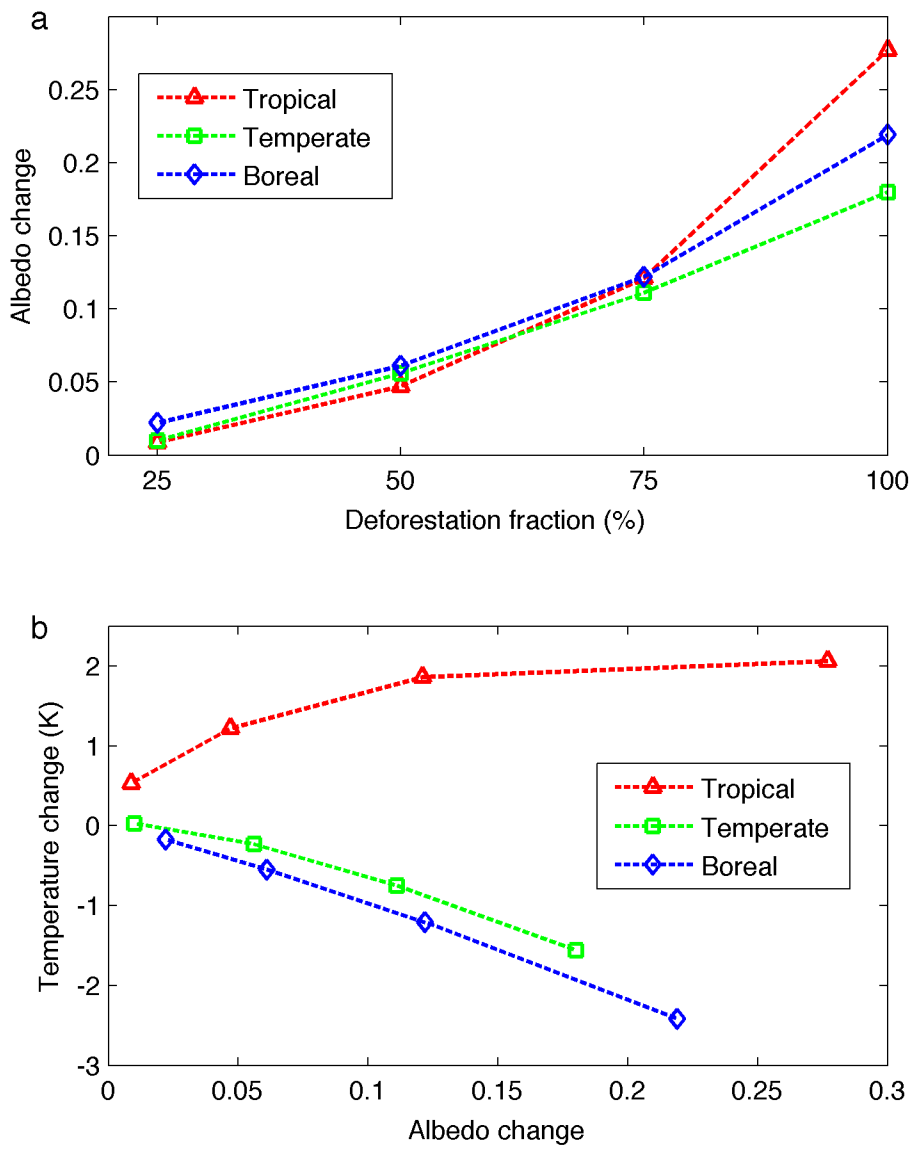
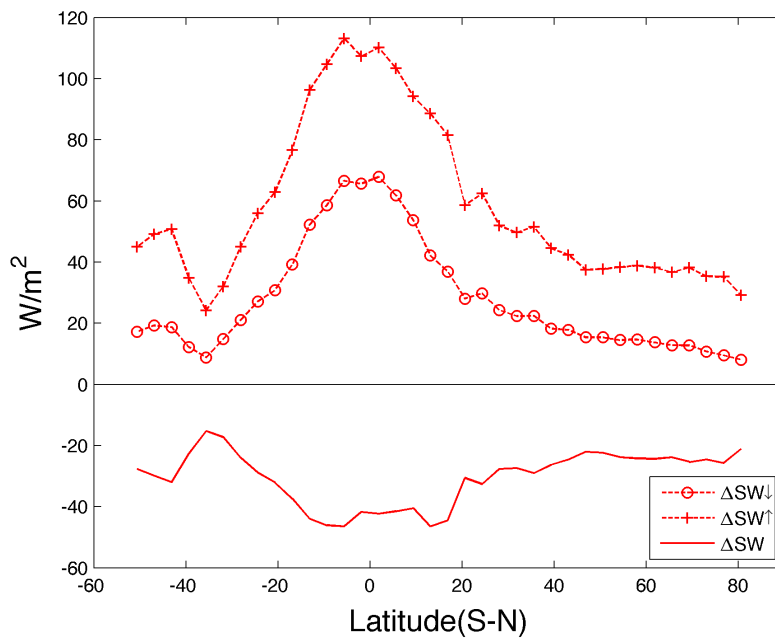


Figure S6. (a) Response of albedo change to growing deforestation fraction from 25% to 100% and (b) temperature response to albedo change under different deforestation fractions. Data points in the figure are from Table 3.

802



803

Figure S7. Latitudinal changes in downward (ΔSW_{\downarrow}), upward (ΔSW_{\uparrow}) and absorbed shortwave radiation (ΔSW)

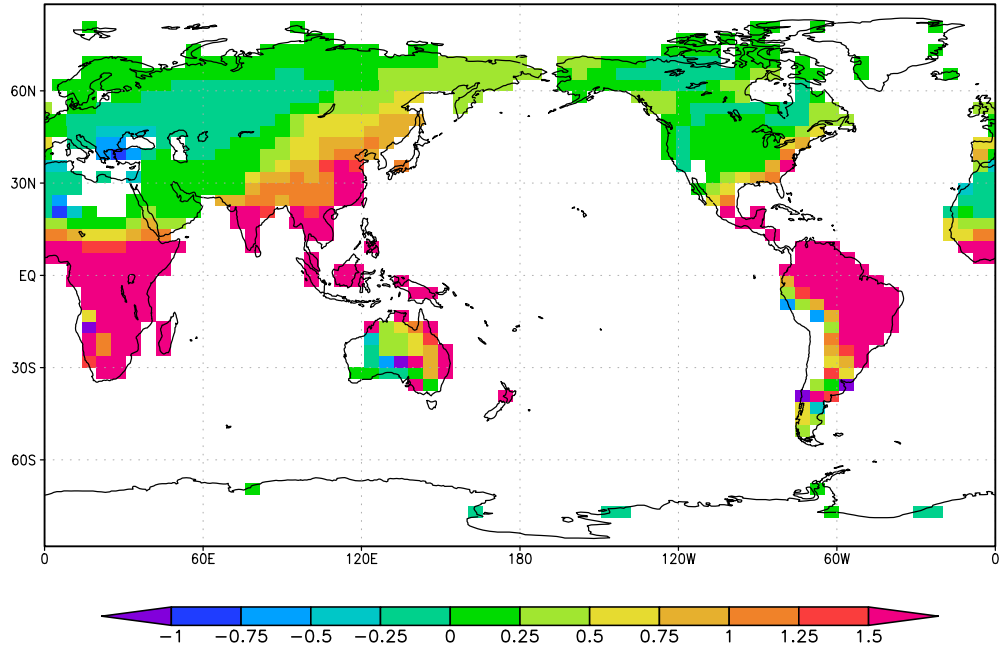
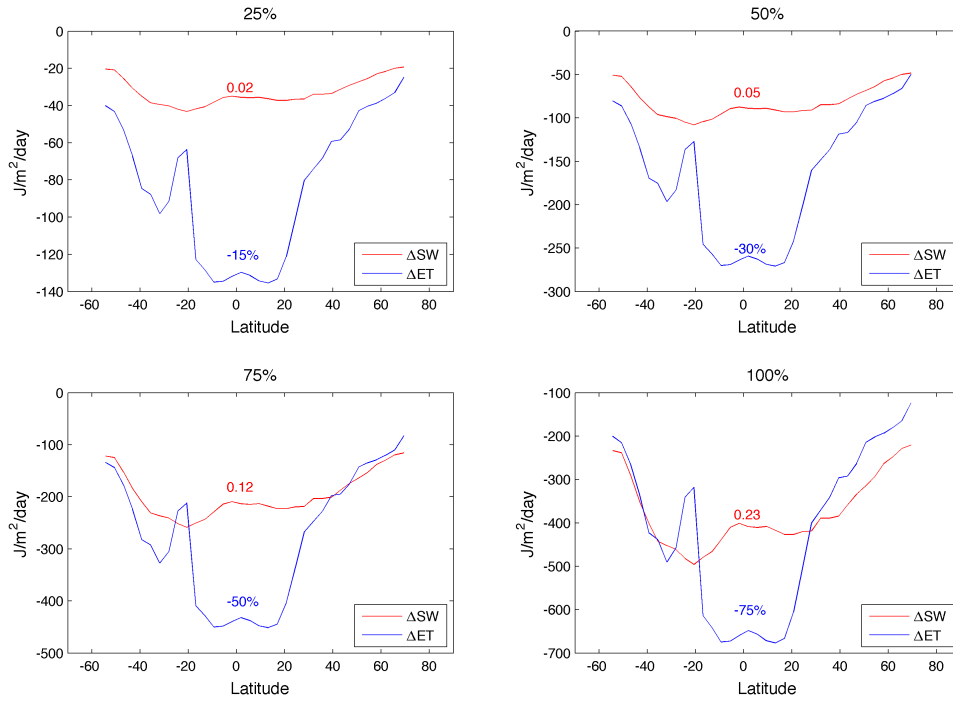


Figure S8. Ratio of $\Delta ET / \Delta SW$ in global deforestation



804

Figure S9. ΔSW and ΔET calculated with MODIS ET and shortwave radiation (data from Li et al. (2015))

805

806

807